

Catalyst shape matters: Influence of catalyst shape on reactor performance in hydrogen release from perhydro benzyltoluene

T. Rüde^a, D. Strauch^a, N. Szesni^b, M. Wolf^c, P. Wasserscheid^{a,d,e}, F. Auer^{a,*}

^a Forschungszentrum Jülich GmbH, Helmholtz-Institute Erlangen-Nürnberg for Renewable Energy (IEK 11), Erlangen, Germany

^b Clariant Produkte Deutschland GmbH, Heufeld, Germany

^c Karlsruhe Institute of Technology (KIT), Engler-Bunte-Institut & Institute of Catalysis Research and Technology, Karlsruhe, Germany

^d Friedrich-Alexander-Universität Erlangen-Nürnberg (FAU), Lehrstuhl für Chemische Reaktionstechnik, Erlangen, Germany

^e Forschungszentrum Jülich GmbH, Institute for a Sustainable Hydrogen Economy (INW), Jülich, Germany

ARTICLE INFO

Handling Editor: Dr M Djukic

Keywords:

Catalyst shape

Pellet geometry

LOHC

Catalytic distillation

ABSTRACT

This study investigates how the geometrical catalyst pellet shape affects the reaction performance in hydrogen release from the liquid organic hydrogen carrier (LOHC) compound perhydro benzyltoluene (H12-BT). A catalytic distillation (CD) reactor setup serves as experimental platform for our investigation of different catalyst pellet shapes in H12-BT dehydrogenation. CD facilitates H₂ release from H12-BT at lower temperatures enabling heat integration of this endothermic process with low temperature waste heat sources. At 200 mbar_{abs} and temperatures below 250 °C, we achieved complete dehydrogenation of H12-BT for the first time. The CD setup enhances the H12-BT concentration in the catalyst bed, but also introduces challenges such as the risk of flooding. Our research introduces a ribbed-ring catalyst shape for the specific purpose of H12-BT dehydrogenation that significantly outperforms the commercial reference catalyst. The ribbed-ring catalyst achieves a 2.4-fold increase in H₂ release rate without additional by-product formation and eliminates the need for a gas channel in the CD thus facilitating scale-up. Liquid phase dehydrogenation (LD) experiments revealed that the superior performance of the ribbed-ring catalyst is mainly due to the increased geometric ratio of outer surface area to pellet volume. Our findings underscore the importance of a tailored catalyst pellet geometry in optimizing fixed-bed reactors for hydrogen release reactions from LOHC systems and other reactions with significant volume expansion.

1. Introduction

During the early stages of catalyst development, attention is primarily centred on improving catalyst activity and selectivity [1]. Yet, if interesting catalyst development candidates are to be scaled-up and applied in continuously operating technical reactors, additional aspects must be taken into account [2].

In larger scale reactors, the geometry of the catalyst pellets becomes a crucial factor as it influences both mechanical strength and hydrodynamic properties in technical operation, e.g., in the typical fixed-bed reactor configuration [2,3]. Catalyst pellets can be produced in different macroscopic shapes [4]. The ideal geometry – often with dimensions in the millimeter range – accomplishes two main objectives: a) it minimizes pore diffusion effects within the catalyst pellets by enhancing the mass transfer area with the surrounding bulk, thereby

improving catalyst utilization [5,6]; b) it limits the pressure drop across the catalyst bed by offering an ideal ratio of catalyst bed volume and void [7]. Despite its significant impact, the geometry of the applied catalyst pellets often receives little attention in literature [1] and has – to the best of our knowledge – not yet been the topic of an LOHC dehydrogenation study so far.

In hydrogen storage technologies using the LOHC concept, commercial spherical catalysts are used to date in the upcoming technical LOHC hydrogenation and dehydrogenation processes [8,9]. In these technologies, hydrogen (H₂) is stored by the reversible hydrogenation and dehydrogenation of a liquid organic compound. The latter is not consumed and can be charged and uncharged many times [6,10]. Recent studies show, that the LOHC technology is particularly interesting for long-term storage or long-distance transport of H₂ compared to other hydrogen storage technologies (such as compression, liquefaction, hydrogenation of CO₂ or N₂) as the diesel-like physicochemical nature of

* Corresponding author. Cauerstr. 1, 91058, Erlangen, Germany.

E-mail address: f.auer@fz-juelich.de (F. Auer).

<https://doi.org/10.1016/j.ijhydene.2025.152174>

Received 16 April 2025; Received in revised form 24 July 2025; Accepted 21 October 2025

Available online 1 November 2025

0360-3199/© 2025 The Authors. Published by Elsevier Ltd on behalf of Hydrogen Energy Publications LLC. This is an open access article under the CC BY license (<http://creativecommons.org/licenses/by/4.0/>).

Abbreviations

CD	Catalytic distillation
DoH	Degree of hydrogenation of the LOHC in %; cf. Equation (1)
H ₂	Hydrogen
H0-BT	Benzyltoluene – LOHC in the form that is not loaded with H ₂ (low DoH)
H12-BT	Perhydro benzyltoluene – LOHC in the form that is loaded with H ₂ (high DoH)
Hx-BT	Benzyltoluene species of varying degree of hydrogenation
ICP-OES	Inductively coupled plasma optical emission spectroscopy
LOHC	Liquid organic hydrogen carrier
MeFl	Methylfluorene content in % summarizing all regioisomers; cf. Equation (2)
p	Pressure
STEM	Scanning transmission electron microscopy
TEM	Transmission electron microscopy
T	Temperature

the LOHC compounds enables the further utilization of the existing fuel infrastructure [11–15]. In the quest of more effective LOHC technologies, the LOHC dehydrogenation reaction, that releases the hydrogen from the carrier, remains in our focus as this reaction has to provide the hydrogen in the highest possible space-time-yield, energetic efficiency, and purity to the customer or to the hydrogen consuming consecutive process step [13,16–18].

Catalytic distillation (CD) is one way to intensify the LOHC dehydrogenation process [19]. CD offers advantages, such as increased H₂ release rates, reduced by-product formation, effective heat provision to the endothermic reaction, and intrinsic separation of hydrogen and discharged LOHC material from the reaction zone thus enhancing the thermodynamic driving force for hydrogen release [19]. This allows effective hydrogen production at low temperatures enabling integration of waste heat from adjacent exothermal processes into the endothermic LOHC dehydrogenation. The viability of various heat sources increases as the temperature level of the LOHC dehydrogenation decreases [20]. In particular, heat integration with high-temperature fuel cells or hydrogen combustion processes appears obvious [21–23] to realize autothermic re-electrification processes of LOHC bound H₂ [24].

CD for LOHC dehydrogenation processes has so far been experimentally proven for the LOHC system benzyltoluene (H0-BT)/perhydro benzyltoluene (H12-BT) [10,25,26]. Note, that for CD the temperature range for the LOHC dehydrogenation reaction must coincide with that of the distillation process [27]. In this way, dehydrogenation of H12-BT has been demonstrated at temperatures down to 200 °C, if the operation was carried out in a reactive distillation column under reduced pressure [19].

In the recent past, catalyst optimization studies have been carried out to develop H12-BT dehydrogenation catalysts that provide fast kinetics at low temperatures. In this context powder catalysts with high platinum dispersions and incorporation of rhenium as a second metallic component proved to boost activity [25,28,29] compared to the commercially used spherical core-shell Pt/Al₂O₃ catalyst (Clariant EleMax D102) that was originally developed for liquid-phase dehydrogenation of perhydro dibenzyltoluene at reaction temperatures of 300 °C [30–33]. To address the vast volume increase due to H₂ gas evolution during LOHC dehydrogenation, the use of coated wall reactors has been discussed in the literature as a possible way for process intensification. But reduced catalyst volume per reactor volume and also coating stability issues have been identified as problematic aspects for this otherwise attractive

approach [34–37].

In this study we focus on a different approach for process intensification that focuses in particular on the low temperature H12-BT dehydrogenation and the optimization of catalyst pellet shape in a CD-based dehydrogenation reactor. CD requires a proper selection of catalyst pellet shape to deal with flooding risks in the counter-current flow of gas and liquid under distillation conditions [38–40]. Conventional spherical catalysts often prove unfavourable [25,40,41] and pellet shapes with a geometry similar to distillation packings appear more promising [42]. Therefore, we have explored the performance of different catalyst pellet shapes in our laboratory CD setup for low-temperature dehydrogenation of H12-BT. In this context we have conducted a comprehensive examination of pellet properties to pinpoint properties that are critical for the hydrogen release performance.

2. Experimental

2.1. Materials

The spherical catalyst Clariant EleMax D102 [8,10,43] is the current state-of-the-art for the dehydrogenation of benzyltoluene-based LOHC systems [32,43] and was therefore used in this study as reference material.

To investigate the influence of different catalyst shapes on reactivity in the CD-based dehydrogenation process, five Pt/Al₂O₃ pellet catalysts were produced in a similar way like the commercial reference by *Clariant Produkte Deutschland GmbH*. Identical to the EleMax D102 material, all catalysts have a target Pt loading of 0.3 %_{wt} and exhibit a core-shell distribution of Pt on the Al₂O₃ support. Additionally, all catalysts were selectively poisoned with trace amounts of sulphur to realize the well-known beneficial effects of such partial poisoning on activity and selectivity [44]. Thereby, platinum sulphite acid solution was used as Pt and S containing precursor for the production of all catalysts, resulting in a molar ratio of Pt:S of nominally 1:2. The different shapes are schematically illustrated in Table 1. Microscopic images of the catalysts in cross-section can be found in Table S-5 of the ESI. For the dehydrogenation experiments, the spheres were divided into a large ($d_{\text{mean}} = 3.5$ mm) and a small ($d_{\text{mean}} = 2.8$ mm) fraction to compare the effect of effective diffusion length on the performance.

The H12-BT used in our dehydrogenation experiments had a degree of hydrogenation $DoH = 98.6$ % and was produced by hydrogenation of H0-BT (*Marlotherm® LH*) purchased from *Eastman Chemical Company* at 300 °C and 30 bar H₂ using a commercial Pt–Pd/Al₂O₃ catalyst (*EleMax H*, *Clariant Produkte GmbH*) in a trickle bed reactor.

2.2. Catalyst characterization

To gain a comprehensive overview on the characteristic properties of the differently shaped catalysts under investigation in this study, various characterization methods were applied to determine their physical, textural and chemical properties (see Table 2).

The calculation of the geometric surface area and of the volume of the shaped catalyst bodies was carried out based on a 3D-CAD model of their different geometries with the Software Autodesk Inventor.

Textural properties were assessed by nitrogen physisorption. Prior to the measurements with a TriStar Plus from Micromeritics, the samples were degassed in vacuum for 12 h at 250 °C. The analysis was carried out at –196 °C and evaluation of the specific surface area was performed using the BET method (relative pressure range: 0.05–0.35). Mean pore diameters were derived from the sorption isotherms with the help of the BJH method, considering ad- and desorption isotherms.

Inductively coupled plasma optical emission spectroscopy (ICP-OES) was used to analyze the targeted catalyst loading of 0.3 %_{wt} Pt. The catalyst samples were ground and dissolved in a concentrated mixture of HCl, HNO₃, HF using microwave digestion. The analysis was carried out with a Ciroc CCD from Spectro Analytical Instruments after calibration

Table 1

Schematic illustration and dimensions of the tested catalyst pellet geometries.

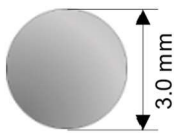
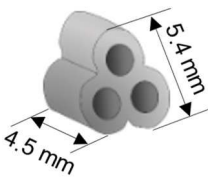
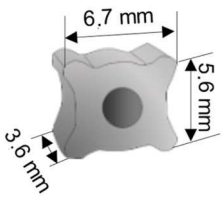
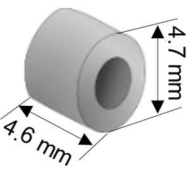
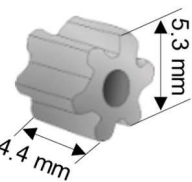
Sphere	Trihole	Double alpha	Ring	Ribbed ring
				

Table 2

Characteristic catalyst/properties that can impact catalytic performance.

Physical properties	Textural properties	Chemical properties
Geometric surface area	BET surface area	Platinum loading
Pellet volume	Mean pore diameter	Platinum particle size
		Platinum shell thickness

with standard solutions of Pt.

Scanning transmission electron microscopy (STEM) images were recorded on a Talos F200i (Thermo Fisher Scientific) operated at a primary electron energy of 200 keV. The samples were prepared by selectively removing catalyst material from the darker shell, grinding and suspending it in isopropanol for drop-casting onto copper TEM grids. For the determination of the mean Pt particle size and the particle size distribution a minimum of 120 particles from various images were analyzed for each catalyst using the software ImageJ [45]. The Pt shell thickness was estimated based on scanning electron microscopy (SEM) images which were taken over the cross-section of the catalyst pellets with a Phenom XL G2 (Thermo Fisher Scientific). Integrated EDX area analysis enabled the identification of the Pt loaded shell of the catalyst pellets. The shell thickness was identified by the contrast indicated by the Pt EDX analysis and derived as a mean value from ten measurements at different positions of the catalyst pellet.

2.3. Dehydrogenation via catalytic distillation (CD)

For the semi-batch CD experiments, a glass column with a diameter of 30 mm and a length of 450 mm was utilized. The general setup and procedure was adopted from Ref. [19]. At the column bottom, a 100 ml flask with a 110 W PILZ laboratory heater (WHG2, Winkler GmbH) was used as reboiler and set to 100 % heating power throughout the experiment. To reduce heat losses, the flask and the connection to the column were wrapped in glass wool. An electric heating jacket around the column together with a microprocessor temperature controller (HT MC1, Horst GmbH) served as insulation. The set point was chosen to mimic the lowest temperature measured within the column to induce near adiabatic conditions. A five-point thermocouple was introduced into the column head through a Bola HT GL 14 laboratory screw joint to record the internal temperature profile via a PicoLog TC-08 data logger. At the column top, a 600 mm long borosilicate glass Dimroth vapor condenser with an internal double spiral through which 17 °C cooling water flows as coolant separated the released H₂ gas stream from the Hx-BT vapor. No condensate was observed downstream of the condenser during any of the experiments. Hx-BT was liquified and according to the principle of total reflux returned to the column by dripping onto the catalyst fixed-bed. Thereby a reflux was established leading to counter-current flow within the column. The condenser was connected to an active carbon filter for removal of impurities from H₂ before the gas was sucked out by a Vacuubrand MD 4C Ex Vario vacuum diaphragm pump. The pressure at the column top was recorded and controlled by the Vacuubrand CVC 3000 vacuum controller. A simplified depiction of the applied CD laboratory setup is found in Figure S-1 of the ESI.

For each experiment, the bottom flask was filled with 45 g of perhydro benzyltoluene (H12-BT) and 400 mm of Pro-Pak® 0.24 separation packing (see ESI for an initial assessment of different packing materials in Figure S-2 and Figure S-5) topped with 15 g of catalyst packing were placed in the column [43]. The catalyst packing was placed in the upper part of the column to exploit the upwards increasing concentration of light-boiling H12-BT under distillation conditions [46]. The molar ratio of the reversibly bound H₂ in H12-BT to the active metal Pt was $n(\text{H}_{2,\text{max}}):n(\text{Pt}) = 12,000:1$ in all experiments. Before heating up, the setup underwent inertization by purging with argon for 10 min. The reaction start was defined by the time at which the first droplet of H12-BT condensed and returned to the catalyst bed. During the runtime, liquid samples were taken from the bottom flask in regular intervals to monitor the reaction progress.

2.4. Liquid phase dehydrogenation at non-distillative conditions (LD)

Semi-batch dehydrogenation experiments in the liquid phase at atmospheric pressure were carried out in a glass setup. A 100 ml five-necked flask was filled with 32.9 g of H12-BT and attached to an intensive condenser ($T = 1.5\text{ °C}$) through the middle neck. An Ar (5.0, Linde) supply line, a Pt100 thermocouple and a catalyst dosing device, filled with the catalyst pellets ($n(\text{H}_{2,\text{max}}):n(\text{Pt}) = 10,000:1$), were connected to the further necks. The remaining neck was sealed with a rubber septum and used for sampling during the reaction. The reaction mixture was magnetically stirred and heated with a PILZ heating mantle, controlled by a Fitron 4 TP temperature controller (Fiege electronics). Before heating, the reaction setup underwent inertization by flushing with an Ar stream. After reaching the reaction temperature of 250 °C, a zero sample was taken, the catalyst was released into the pre-heated LOHC, and the reaction time was started. Further liquid samples were taken after 30, 60, 120, 240 and 1320 min with the help of a 1 ml syringe and cannula through the septum.

2.5. LOHC product analysis

The liquid LOHC samples were analyzed by refractometry and gas chromatography (GC). Refractometry served for immediate monitoring of the reaction progress using a method described by Aslam [47] that was adapted to the H0-BT/H12-BT LOHC system [25]. The degree of hydrogenation DoH and the purity of the liquid samples were determined offline by analysis with a Trace 1310 gas chromatograph (GC) from Fisher Scientific equipped with a Rxi17Sil column (30 m length; 250 µm inner diameter). The procedure was adopted from Ref. [10] (details can be found in the ESI). The DoH of the sample was calculated according to Equation (1) with the weighted GC-peak areas A of the three Hx-BT species. The content of methylfluorene $MeFl$ and, analogously, that of H0-BT, H6-BT, and H12-BT was derived from the corresponding GC-peak area ratio in Equation (2).

$$DoH \text{ / } \% = \frac{100\% \cdot A_{H12-BT} + 50\% \cdot A_{H6-BT}}{A_{H12-BT} + A_{H6-BT} + A_{H0-BT} + A_{MeFl}} \quad (1)$$

$$MeFl / \% = \frac{A_{MeFl}}{A_{H12-BT} + A_{H6-BT} + A_{H0-BT} + A_{MeFl}} \quad (2)$$

2.6. Performance indicators

The catalytic activity of a catalyst at given reaction conditions is indicated by its productivity. We define productivity as the mass of H₂ release per mass of platinum and time. To account for the fact that productivity is a function of reactant concentration and DoH, the productivities in our semi-batch experiments are determined in the DoH range 90–50 % (catalytic distillation, CD) and 90–70 % (liquid phase reaction, LD) according to Equation (3) for the comparison of different catalysts.

$$P / \frac{g_{H_2} \cdot g_{Pt}^{-1} \cdot \min^{-1}}{m_{Pt} \cdot (t_{50/70\%} - t_{90\%})} = \frac{m_{H_2, \max} \cdot (90\% - 50/70\%)}{m_{Pt} \cdot (t_{50/70\%} - t_{90\%})} \quad (3)$$

The maximum mass of reversibly bound H₂ in the LOHC, $m_{H_2, \max}$, is calculated via the total amount and the initial DoH of the applied H12-BT. The platinum mass m_{Pt} was determined by multiplication of the catalyst weight with its platinum loading as measured by ICP-OES. The characteristic times for a DoH of 50 %, 70 % and 90 % are labelled t_{50} , t_{70} and t_{90} , respectively. These are determined by fitting or interpolating the DoH from GC analysis as a function of time. A numerical ODE solver and least squares minimization with a power law model [48,49] or Catmull-Rom interpolation [50] were employed for this purpose.

3. Results and discussion

3.1. Catalyst characterization

To pinpoint the performance differences between catalysts of various geometries, we thoroughly characterized them and compared their properties (Table 3). ICP-OES analysis confirmed the targeted Pt loading of $(0.3 \pm 0.05)\%_{wt}$ for all catalyst materials.

Porosity of the catalyst packing (voidage) is a key factor influencing pressure drop in fixed beds. Compared to spheres ($\sim 45\%$ void), shaped carriers offer $\geq 55\%$ void space, facilitating better gas and liquid flow. Pellet lengths range from 2 to 4.6 mm. Trihole, double-alpha, and ring shapes show low length variation due to tableting, whereas granulated spheres and extruded ribbed rings are less uniform and less dense. The geometric surface area (outer surface area), which determines the accessibility of the active catalyst shell and also its thickness [51,52], is significantly smaller for the spherical catalyst material compared to the applied trihole, double alpha, ring, and ribbed ring materials. Interestingly, the expected correlation that higher geometric surface area leads to thinner catalyst shells is not shown by the experimental data. The specific surface area (inner surface area), which should influence the dispersion and size of the active metal nanoparticles [53], spreads

between 99 (trihole) and 207 m² g^{−1} (ring). Closely related to the specific surface area is the mean pore diameter of the catalyst material [54] which covers a range between 7 (spheres) and 13 nm (trihole). The nanoparticle size, which determines the share of exposed Pt surface atoms [55], was found within the range of 1.1 (trihole) to 1.6 nm (double alpha).

3.2. Pellet shape variation in H₂ release at low temperature using CD

The first CD dehydrogenation experiments with H12-BT were conducted with the commercial catalyst EleMax D102. Until now, there was no demonstration of complete H₂ release from H12-BT, even though this is possible from a thermodynamic point of view [20]. In theory, the boiling LOHC in the CD lowers the H₂ partial pressure significantly while the semi-batch operation mode continuously drives the equilibrium to the product side. However, this thermodynamic consideration does not take the slow kinetics at the applied low reboiler temperatures and other limiting factors, such as possible inhibition of H₂ bubble nucleation [56], into account. This makes experimental validation necessary.

The first CD experiments were conducted at 200 mbar_{abs} with a wire mesh gas channel ($d = 10$ mm) placed in the column to suppress flooding of the reaction section despite the little interparticular void and the low gas density under operating conditions [19]. This low pressure leads to a maximum reboiler temperature of below 240 °C, a temperature at which heat integration, e.g. with a high temperature PEM fuel cell or the exhaust gas of a hydrogen engine or turbine, comes into reach [24,57, 58].

Fig. 1 shows the DoH during an extended CD experiment over more than five days. After 5800 min more than 99 % of the reversibly bound H₂ was released from H12-BT. Thorough GC analyses revealed that more than 99.8 % H₂ release was achieved after 7200 min of operation. Such an extremely deep dehydrogenation is unprecedented in literature, even for higher reaction temperatures. This result remarkably highlights the potential of a CD process for LOHC dehydrogenation. The complete dehydrogenation was validated in four individual repetitions. The reproducibility was excellent with an average absolute error (AAE) between the experimental data points and a simple fitted kinetic model of only 0.014 (see Figure S-3 in the ESI for details).

The GC analysis reveals further details about reactant depletion and the formation of reaction intermediates, products, and by-products (see Fig. 2). For the compound H12-BT a monotonous conversion can be observed, approaching near-complete depletion over the first 3000 min. H6-BT is formed as an intermediate with a maximum molar share of approx. 60 % in the reaction mixture at around 1400 min. At this point H0-BT formation is observed and, after a monotonous increase, reaches a plateau at a share of about 90 % after 4500 min.

Previously, methylfluorene regioisomers formed by a consecutive dehydrogenation of H0-BT were identified as main by-products of H12-

Table 3

Physical, textural and chemical properties of the herein applied pellet catalysts of different geometrical shapes.

Catalyst shape	Spheres large	Spheres small	Trihole	Double alpha	Ring	Ribbed ring
Geometric surface area ^a /mm ²	40	25	181	167	125	166
Pellet volume ^b /mm ³	24	12	72	107	63	66
Pellet length/mm	2.00 – 4.00	4.45 ± 0.03	3.59 ± 0.06	4.62 ± 0.06	4.39 ± 0.22	
	∅ 3.50	∅ 2.80				
Packing porosity (voidage) ^b /-	0.45	0.58	0.58	0.55	0.61	
Specific surface area ^c /m ² g ^{−1}	157	99	102	207	107	
Mean pore diameter ^c /nm	7	13	11	8	12	
Mean Pt particle diameter ^d /nm	1.2	1.1	1.6	1.2	1.4	
Mean Pt shell thickness ^e /μm	16 ± 3	35 ± 2	32 ± 3	41 ± 3	20 ± 5	

^a per catalyst pellet.

^b determined in a 20 ml snap cap vial.

^c as determined by means of nitrogen physisorption and the BET/BJH method (see also Table S-2 in the ESI).

^d based on size analysis via TEM (see also Table S-3 in the ESI).

^e based on SEM-EDX (see also Table S-4 in the ESI).

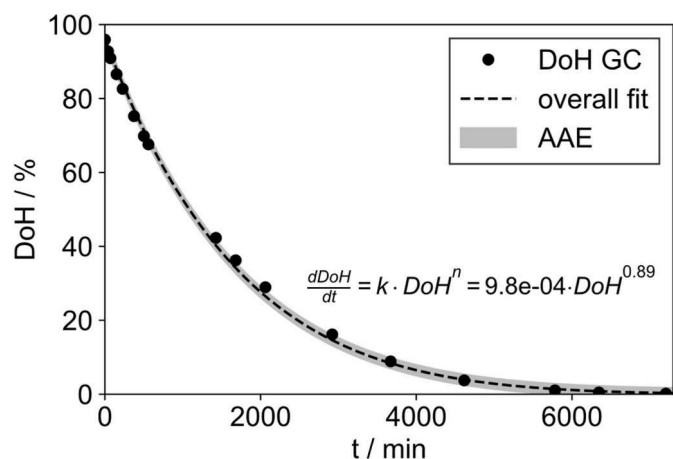


Fig. 1. Extended CD run with the commercial EleMax D102 catalyst for the dehydrogenation of H12-BT indicated by *DoH* over reaction time; ($p = 200$ mbar_{abs}, $h_{\text{ProPak}} = 400$ mm, $m_{\text{catalyst}} = 15.05$ g, 0.3 %_{wt} Pt/ Al_2O_3 , $m_{\text{H12-BT}} = 45$ g); the grey region around the black dashed line indicates the average absolute error (AAE) of the measured data points from four reproductions to a fitted power law model.

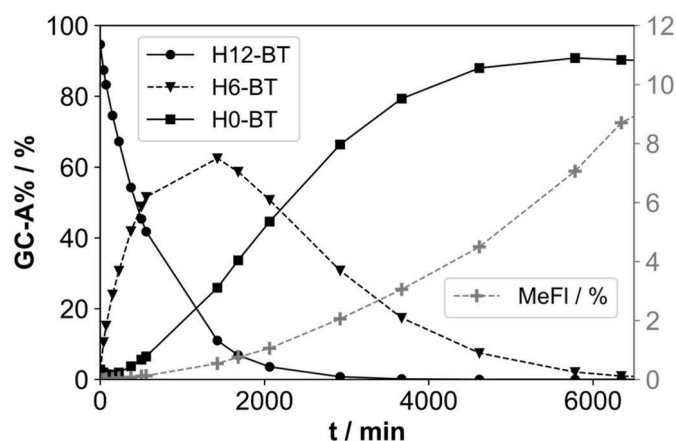


Fig. 2. Reaction mixture composition during an extended CD run with the commercial EleMax D102 catalyst in the dehydrogenation of H12-BT. The graph shows the consumption of H12-BT, the formation and depletion of the intermediate H6-BT as well as product H0-BT and the by-product MeFl formation. Reaction conditions: $p = 200$ mbar_{abs}, $h_{\text{ProPak}} = 400$ mm, $m_{\text{catalyst}} = 15.05$ g, 0.3 %_{wt} Pt/ Al_2O_3 , $m_{\text{H12-BT}} = 45$ g.

BT dehydrogenation [10]. Methylfluorene regioisomers themselves can store hydrogen and retain the storage capacity of the LOHC system, but their formation should be limited due to their high melting point and potential impact on the recyclability of LOHC material [10]. *MeFl* increases gradually from zero to almost 8 % in the product mixture after 6200 min. From Fig. 2 one can expect that with even longer reaction times, H0-BT would slowly convert to methylfluorene which represents a viable LOHC compound itself [59,60].

Over the course of the experiment, the pressure was controlled precisely and remained at (200.1 ± 0.5) mbar_{abs}. The temperature in the catalyst bed increased gradually from approx. 200 to 215 °C during the dehydrogenation reaction (see Figure S-4 in the ESI for details). This temperature rise is directly linked to the semi-batch operation of the CD process and to the formation of H0-BT, which has a higher boiling point than H12-BT and accumulates in the catalyst bed with increasing reaction progress. Furthermore, the temperature profile (see Figure S-4 in the ESI) over the column height reflects the effectiveness of the separation with Pro-Pak, where lighter boiling products accumulate towards

the top of the column.

Besides the demonstration of complete dehydrogenation by the CD process, the high reproducibility of the experimental setup and procedure indicates very good process stability. This establishes a reliable basis for comparing the performance of differently shaped catalyst pellets in the CD. Given the complex hydrodynamics in the operating CD process with counter-current flow of gas and liquid in a catalyst bed producing high gas volumes, the observed process stability is highly encouraging.

3.3. Variation of the catalyst pellet shape in CD

To evaluate the influence of different catalyst pellet geometries on the catalytic performance in the CD process, rings, ribbed rings, triholes, and double alpha (see Table 1) were tested and compared with the commercial spherical EleMax D102 benchmark catalyst. The catalyst benchmark experiment was reproduced thrice and it can be deduced that the uncertainty of ± 4.9 % indicated by the error bar in Fig. 3 is likely to be comparable for all of the tested catalysts. The first major advantage is that these more complex shapes with high packing porosity (voidage) do not require a gas channel in the CD process which is only required for spherical catalysts to prevent flooding [61,62]. This increases the useable volume for the catalytic reaction in the column and is a major step towards scale-up of CD in hydrogen release reactions from LOHC systems. Note that these non-spherical shaped catalysts are still cost-effective to manufacture and allow for easy handling compared to structured packings [39,63] as they provide good mechanical stability and can be simply filled into the reactor as bulk material [40]. Fig. 3 compares the productivity of the various catalyst pellet shapes in the CD setup for the range of *DoH* = 90–50 %.

The triholes and the double alpha catalyst pellets showed a lower dehydrogenation performance in comparison to the commercial benchmark EleMax D102. The rings and especially the ribbed rings outperformed the benchmark catalyst by far. With the ribbed ring catalyst, a 2.4 times higher productivity was achieved compared to the technical benchmark. Also, with the ribbed ring catalyst the temperature in the catalyst bed was confirmed to be as low as (200.1 ± 0.3) °C. Astonishingly and despite the low temperature, the ribbed rings achieved a *DoH* of 1 % after just 1480 min (see *DoH* over time in Figure S-6 of the ESI).

To verify the performance of the ribbed rings, the semi-batch CD experiment was repeated with half the catalyst mass to target a similar H_2 release and similar fluid dynamics compared to the other shaped catalysts. The distillation packing was extended to achieve the same

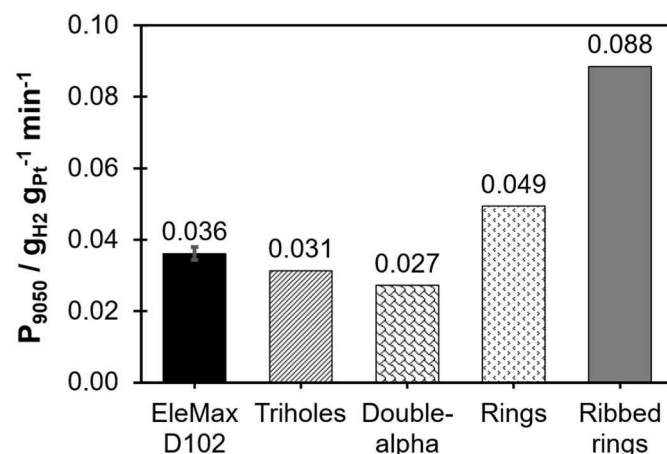


Fig. 3. Comparison of the productivities of the commercial benchmark EleMax D102 catalyst with four non-spherically shaped pellet catalysts in our laboratory semi-batch CD ($p = 200$ mbar_{abs}, $h_{\text{ProPak}} = 400$ mm, $m_{\text{catalyst}} = 15.05$ g, 0.3 %_{wt} Pt/ Al_2O_3 , $m_{\text{H12-BT}} = 45$ g).

overall packing height. Expectedly, the power density based on the internal column volume was halved. However, the Pt-based productivity was even slightly higher with $0.095 \text{ g}_{\text{H}_2} \text{ g}_{\text{Pt}} \text{ min}^{-1}$ in the case with half the catalyst volume. This may be due to the improved separation with the 11 % higher Pro-Pak distillation packing in this case. When referring the *DoH* of both experiments to the time per mass of catalyst (see Figure S-7 in the ESI), the performance becomes almost identical underlining the good reproducibility of the CD setup.

Additionally, the by-product formation was analyzed by GC. In Figure S-8 in the ESI the measured *MeFl* is plotted as a function of the H₀-BT molar fraction. For all catalysts, *MeFl* increased slowly and almost linearly with the H₀-BT fraction up to a concentration of H₀-BT of approx. 80 %. For higher concentrations of H₀-BT, *MeFl* formation increases sharply and exceeds 0.5 %. The rings and the double alpha pellets were found to form the same amount of by-product as the EleMax D102 benchmark. The triholes and the ribbed rings exhibited lower by-product formation, considering the measurement uncertainty. One possible explanation for the reduced by-product formation with the ribbed rings catalyst is the generally accelerated dehydrogenation, which minimizes the contact time of catalyst with H₀-BT leading to a lower probability for deep dehydrogenation to *MeFl*. Other high boilers beyond the *MeFl* peaks in the GC hardly increased during the whole dehydrogenation experiments. Overall, none of the shaped catalysts had disadvantages regarding by-product formation in comparison to the commercial benchmark, again the ribbed rings proved to be particularly advantageous.

To further illustrate the rapid dehydrogenation using ribbed rings, Fig. 4 shows the productivities related to consecutive liquid samples for the experiments with 7.5 and 15 g ribbed rings catalyst in the column. These are compared to the commercial EleMax D102 catalyst. As expected, the initial productivity of the ribbed ring catalyst was with $0.12 \text{ g}_{\text{H}_2} \text{ g}_{\text{Pt}} \text{ min}^{-1}$ about twice as high as that of EleMax D102. Over the whole *DoH* range, the ribbed rings achieved substantially higher productivities and formed less by-products.

Several reasons may be relevant to explain the superior performance of the ribbed ring catalyst material in the CD experiments. The activity differences could be due to different flow patterns in the gas and liquid counter-current flow of the CD. However, these differences are difficult to assess experimentally and computational flow dynamic simulations for reactive three-phase systems with strong volume change are still deficient [64–67]. Therefore, we decided to perform additional liquid phase dehydrogenation experiments in a stirred glass flask with these shaped catalysts as well as their ground analogues to shed more light on the observed differences in the catalytic performance.

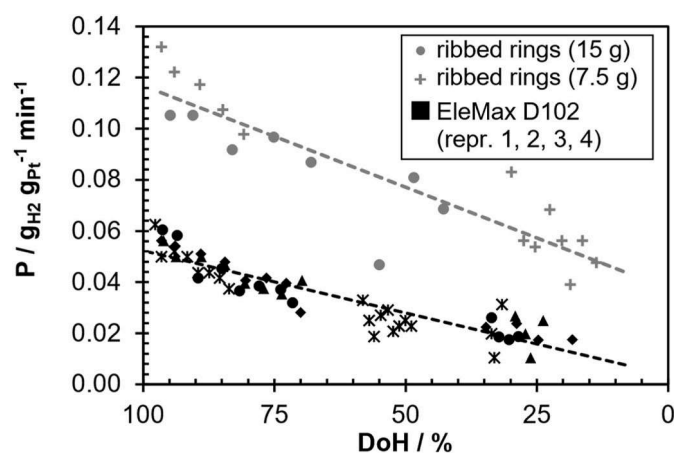


Fig. 4. Productivity of all reproductions including those with half the catalyst mass as a function of the *DoH* for the laboratory semi-batch CD; ($p = 200 \text{ mbar}_{\text{abs}}$, $h_{\text{ProPak}} = 400 \text{ mm}$, $m_{\text{catalyst}} = 15.05 \text{ g}$, $0.3 \text{ \%}_{\text{wt}} \text{ Pt/Al}_2\text{O}_3$, $m_{\text{H12-BT}} = 45 \text{ g}$).

3.4. Liquid phase dehydrogenation (LD) to clarify catalyst shape effects

Fig. 5 presents the catalyst productivities in liquid phase, semi-batch dehydrogenation experiments for the various catalyst shapes. All catalyst shapes are compared at a *DoH* range of 90–70 %, in addition EleMax D102 is also shown as the commercial standard.

Interestingly, the dehydrogenation productivities of the differently shaped catalyst pellets exhibit in the liquid phase semi-batch experiments a similar order than found under CD operation. Again, the ribbed ring material is the most productive, reaching 1.4 times higher productivity than the commercial EleMax D102 standard (under CD conditions the factor was 2.4). This leads us to the conclusion that apart from hydrodynamic aspects under CD conditions there is also a beneficial effect of the ribbed ring shape of the catalyst under the classical liquid phase dehydrogenation conditions.

To exclude effects by textural and chemical properties of the investigated ribbed ring catalyst, we decided to grind all catalysts to a fine powder and test these powders in LD dehydrogenation experiments. This comparison should eliminate all effects induced by the geometrical shape of the original pellets. The results are shown in Fig. 6.

The remarkable finding of these experiments is that all catalyst materials showed the expected difference in dehydrogenation activity for the shaped and the ground form of the catalyst reflecting some degree of pore diffusion limitation except for the ribbed ring catalyst. For the latter, there is nearly no activity difference between pellet and powder form which indicates minimal pore diffusion influence in the shaped ribbed ring material under these liquid-phase dehydrogenation conditions. These comparative experiments indicate the highest influence of pore diffusion on the large spheres and double alpha pellets and a lower influence for the small spheres, triholes and rings. This is well in line with the productivity order for the shaped catalysts shown in Fig. 5.

The influence of diffusional mass transport within a catalyst pellet on the observed reaction rate depends on the characteristic diffusion lengths. This geometric parameter can be approximated by the ratio of pellet volume and geometric surface area (outer surface area of the catalyst pellets). Thereby, a larger geometric surface area at given catalyst volume reduces the risk for a pore diffusion limitation of the dehydrogenation reaction under investigation [68]. According to this consideration, the ratio of geometric surface area *A* and pellet volume *V* were calculated for the different catalyst geometries. These values were then correlated to the productivity ratios between pellet and powder catalysts for the *DoH* range of 90–70 % (Fig. 7).

Indeed, Fig. 7 shows a linear correlation between the *A:V* ratio and the productivity ratio of pellet:powder catalyst is observed. At a larger *A:V* ratio, less diffusional limitation, higher observed dehydrogenation activities and a less pronounced difference between pellet and powder catalyst activity are observed at otherwise very comparable conditions (for details regarding diffusional limitations see ESI). From the presented results, the ribbed ring catalyst shape proves particularly suitable

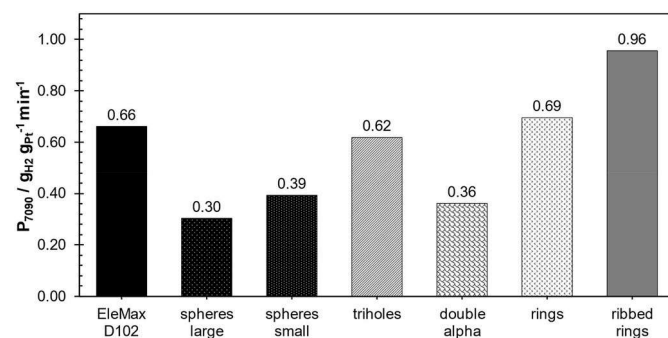


Fig. 5. Productivities of various catalyst pellet shapes in the semi-batch, liquid phase dehydrogenation of H12-BT. Experimental conditions: $T = 250 \text{ }^\circ\text{C}$, $p = 1 \text{ bar}_{\text{abs}}$, $m_{\text{H12-BT}} = 32.9 \text{ g}$, $n_{\text{Pt}}:n_{\text{H12-BT}} = 1:10,000$.

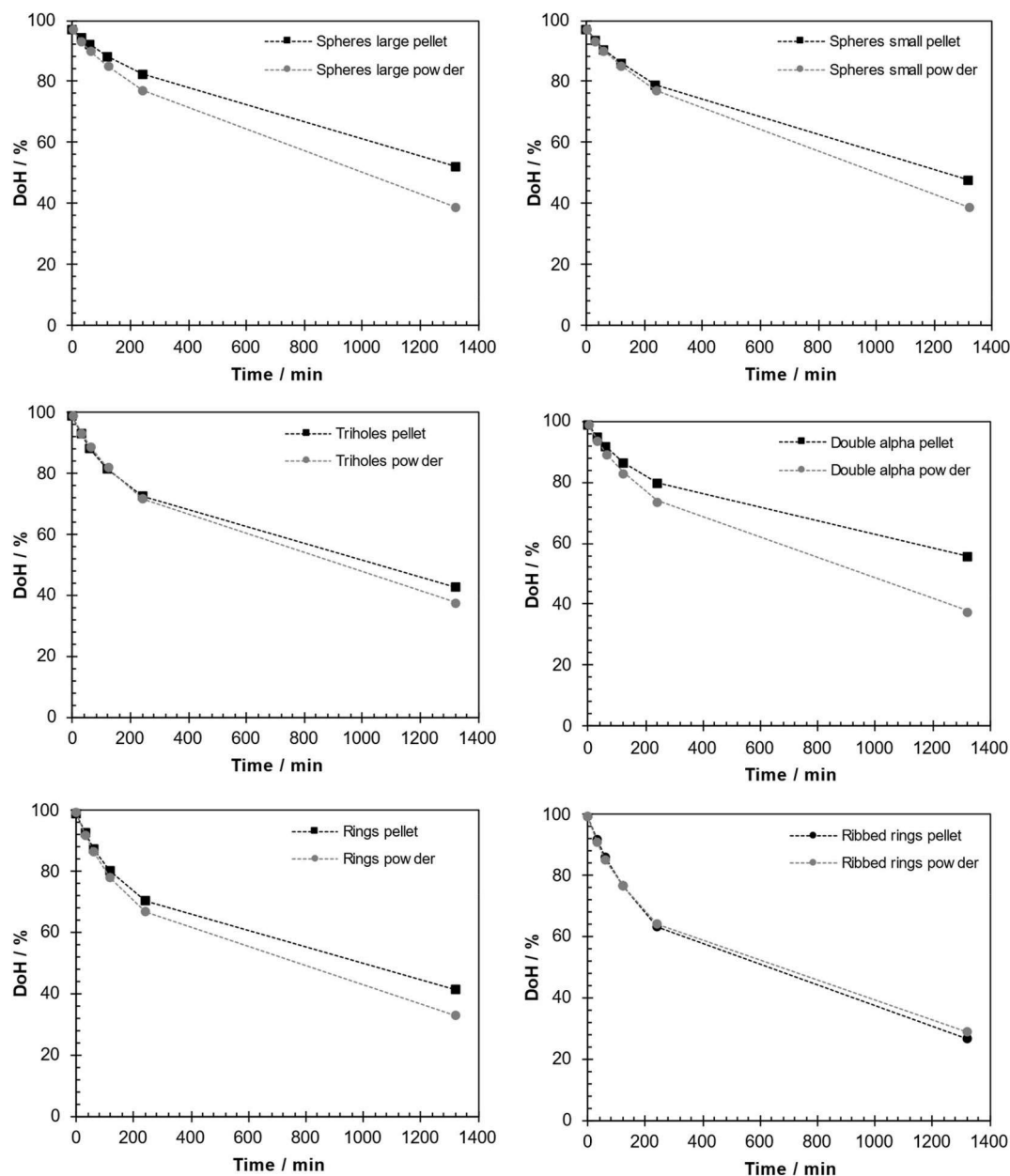


Fig. 6. DoH over time in semi-batch, liquid phase dehydrogenation of H12-BT using shaped catalyst pellets with different geometries and their corresponding catalyst powders after grinding. Experimental conditions: $T = 250\text{ }^{\circ}\text{C}$, $p = 1\text{ bar}_{\text{abs}}$, $m_{\text{H12-BT}} = 32.9\text{ g}$, $n_{\text{Pt}}:n_{\text{H12-BT}} = 1:10,000$.

for the dehydrogenation of H12-BT as it exhibits an extraordinarily large ratio of geometric surface area to pellet volume. This shape is followed by the trihole which is associated with the second largest A:V ratio and correspondingly a productivity ratio near 1.

3.5. Comparison of H12-BT dehydrogenation in CD and LD operation

Finally, we compare the catalytic performance of the investigated shaped catalysts – trihole, double alpha, ring and ribbed ring – with the commercial reference for both CD and LD operation of the H12-BT dehydrogenation reaction. Fig. 8 illustrates that neither the catalyst in trihole nor in double alpha shapes reach the productivity of EleMax D102 in both CD and LD operation mode. Rings and ribbed rings, in contrast, show higher productivities than the commercial standard in both CD and LD. The comparison also suggests that pellet shapes that diverge more distinctly from the spherical reference show stronger performance deviation between CD and LD operation mode. This

observation implies that additional factors, such as beneficial hydrodynamic effects on the counter-current CD operation, amplify the diffusional effects of a high geometric surface to pellet volume ratio on the catalyst productivity. Overall, the ribbed ring shape allows for improved catalytic performance especially in the CD because it is associated with the highest packing voidage values (61 %) and the highest A:V ratio (2.5). This combination opens up the possibility to realize a wide range of fluid flows without flooding the column while simultaneously enabling a fast mass transfer of reactants to and from the active sites.

4. Conclusion

The role of catalyst pellet geometries on the performance in hydrogen release from the charged LOHC-compound H12-BT has been analyzed. Our study has compared shape effects for both catalytic dehydrogenation in catalytic distillation (CD) and in liquid phase dehydrogenation (LD). Two major effects of catalyst pellet shape were

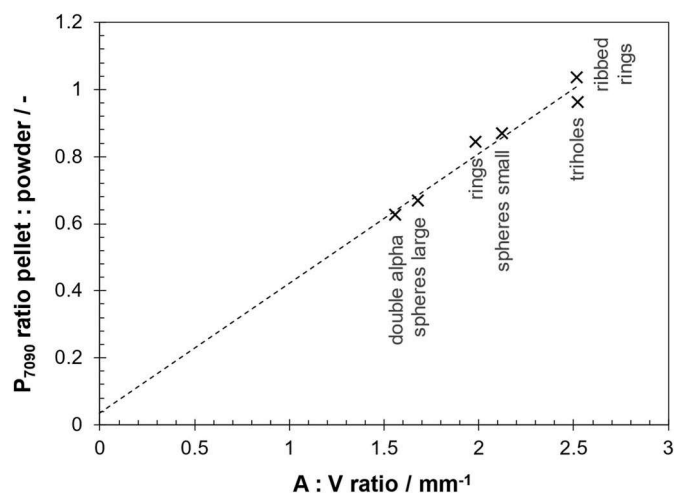


Fig. 7. Correlation between H12-BT liquid phase dehydrogenation productivity in the DoH range of 90-70 % for pellets vs. powder with the A to V ratio (geometric surface to catalyst pellet volume) of the respective shaped catalyst pellets.

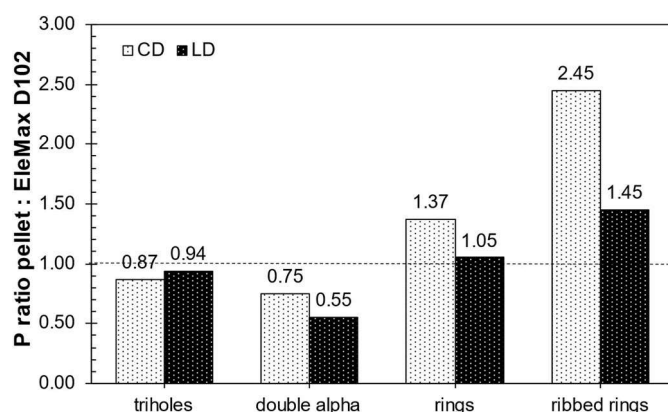


Fig. 8. Comparison of the productivity in H12-BT dehydrogenation using CD or LD operation mode for differently shaped catalyst pellets against the commercial benchmark EleMax D102. Experimental conditions CD: $p = 200 \text{ mbar}_{\text{abs}}$, $h_{\text{ProPak}} = 400 \text{ mm}$, $m_{\text{catalyst}} = 15.05 \text{ g}$, $0.3 \text{ \%}_{\text{wt}} \text{ Pt}/\text{Al}_2\text{O}_3$, $m_{\text{H12-BT}} = 45 \text{ g}$; Experimental conditions LP: $T = 250 \text{ }^\circ\text{C}$, $p = 1 \text{ bar}_{\text{abs}}$, $m_{\text{H12-BT}} = 32.9 \text{ g}$, n_{Pr} : $n_{\text{H12-BT}} = 1:10,000$.

identified in our work: a) The shape influences the accessible external surface area in relation to the pellet volume and thus the degree of pore diffusion limitation effects in the H12-BT dehydrogenation reaction; b) The shape influences the void space in the reactor under operating conditions or the density of catalyst packing in the reactor.

CD operation is affected by a) and b) because the need for high geometric surface area to reduce pore diffusion limitation is complemented by the necessity of maintaining ample void space to reduce flooding risk under distillation conditions with complex gas-liquid counter-current hydrodynamics. LD operation, in contrast, is only affected by a) with, again, the higher geometrical surface area to pellet volume ratio reducing the risk for pore diffusion limitation.

Using the CD operation mode with a reboiler temperature of $240 \text{ }^\circ\text{C}$, our experimental studies showed for the first-time complete dehydrogenation for a heteroatom-free LOHC system (H12-BT) at catalyst bed temperatures below $215 \text{ }^\circ\text{C}$ in excellent reproducibility. Our variation of catalyst shape (spherical state-of-the-art, trihole, double alpha, ring and ribbed ring) showed that non-spherical catalyst shapes made the use of a gas channel against flooding unnecessary. Regarding catalyst performance in CD dehydrogenation mode, the ribbed ring catalyst shape

exhibited the best performance with a 2.4-fold increase in hydrogen release productivity P_{9050} compared to the spherical commercial benchmark EleMax D102. The ribbed ring catalyst achieved almost complete dehydrogenation in about $\frac{1}{4}$ of the time necessary with the commercial benchmark without compromising on by-product formation.

The findings of this study highlight the potential for performance optimization in H12-BT dehydrogenation and similar hydrogen release reactions with large volume change by tailoring catalyst pellet shapes. Future developments may include catalyst pellet shapes with even higher geometric surface area to catalyst pellet volume ratios and pellet geometries optimized by detailed hydrodynamic simulations.

CRediT authorship contribution statement

T. Rüde: Writing – original draft, Visualization, Validation, Methodology, Investigation, Formal analysis, Data curation, Conceptualization. **D. Strauch:** Investigation, Formal analysis, Data curation, Conceptualization. **N. Szesni:** Writing – review & editing, Validation, Conceptualization. **M. Wolf:** Writing – review & editing, Validation, Supervision, Project administration, Conceptualization. **P. Wasserscheid:** Writing – review & editing, Supervision, Resources, Project administration, Funding acquisition, Conceptualization. **F. Auer:** Writing – original draft, Visualization, Validation, Supervision, Project administration, Formal analysis, Data curation, Conceptualization.

Conflicts of interest

Peter Wasserscheid is founder and minority shareholder of the company Hydrogenious LOHC technologies (www.hydrogenious.net) that offers commercially hydrogen storage systems based on the LOHC technology. There is no conflict of interest to declare with regard to the specific scientific results reported in this paper.

Declaration of competing interest

The authors declare the following financial interests/personal relationships which may be considered as potential competing interests: Peter Wasserscheid is founder and minority shareholder of the company Hydrogenious LOHC technologies (www.hydrogenious.net) that offers commercially hydrogen storage systems based on the LOHC technology. There is no conflict of interest to declare with regard to the specific scientific results reported in this paper.

Acknowledgements

This work was funded by the Bavarian Ministry of Economic Affairs, Regional Development and Energy through the project “*Erforschung und Entwicklung eines emissionsfreien und stark emissionsreduzierten Antriebs-systems am Beispiel des Schienenverkehrs*”. The authors would like to thank Dr. Andreas Hutzler, Ana de Oliveira, Nicolas Johnner, Florian Erler and Andreas Müller for their help with the experiments and the characterization of the catalyst samples.

Appendix A. Supplementary data

Supplementary data to this article can be found online at <https://doi.org/10.1016/j.ijhydene.2025.152174>.

References

- [1] Gallei EF, Hesse M, Schwab E. 2.1 development of industrial catalysts. In: Ertl G, Knözinger H, Schüth F, Weitkamp J, editors. Handbook of heterogeneous catalysis. second ed. Weinheim: Wiley-VCH; 2008. p. 57.
- [2] Prieto G, Schüth F. The Yin and Yang in the development of catalytic processes: catalysis research and reaction engineering. Angew Chem Int Ed 2015;54:3222–39.

- [3] Gallei E, Schwab E. Development of technical catalysts. *Catal Today* 1999;51: 535–46.
- [4] Schmidt F. 3.1.3.10 morphological characteristics. In: Ertl G, Knözinger H, Schüth F, Weitkamp J, editors. *Handbook of heterogeneous catalysis*. second ed. Wiley; 2008.
- [5] Afandizadeh S, Foumeny EA. Design of packed bed reactors: guides to catalyst shape, size, and loading selection. *Appl Therm Eng* 2001;21:669–82.
- [6] Jess A, Wasserscheid P. *Chemical technology: from principles to products*. Weinheim: Wiley-VCH; 2020.
- [7] Schüth F, Hesse M. 2.5.2 catalyst forming. In: Ertl G, Knözinger H, Schüth F, Weitkamp J, editors. *Handbook of heterogeneous catalysis*. second ed. Weinheim: Wiley-VCH; 2008. p. 676–99.
- [8] Geiling J, Wagner L, Auer F, Ortner F, Nuß A, Seyfried R, et al. Operational experience with a liquid organic hydrogen carrier (LOHC) system for bidirectional storage of electrical energy over 725 h. *J Energy Storage* 2023;72:108478.
- [9] Kadar J, Gackstatter F, Ortner F, Wagner L, Willner M, Preuster P, et al. Boosting power density of hydrogen release from LOHC systems by an inverted fixed-bed reactor design. *Int J Hydrogen Energy* 2024;59:1376–87.
- [10] Rüde T, Dürr S, Preuster P, Wolf M, Wasserscheid P. Benzyltoluene/perhydro benzyltoluene – pushing the performance limits of pure hydrocarbon liquid organic hydrogen carrier (LOHC) systems. *Sustain Energy Fuels* 2022;6:1541–53.
- [11] Niermann M, Drünert S, Kaltschmitt M, Bonhoff K. Liquid organic hydrogen carriers (LOHCs) – techno-economic analysis of LOHCs in a defined process chain. *Energy Environ Sci* 2019;12:290–307.
- [12] Runge P, Sölch C, Albert J, Wasserscheid P, Zöttl G, Grimm V. Economic comparison of electric fuels produced at excellent locations for renewable energies: a scenario for 2035. 2020. Available at: SSRN.
- [13] Roland-Berger-GmbH. *Hydrogen transportation | the key to unlocking the clean hydrogen economy*. 2021.
- [14] Narayanan TM, He G, Gencer E, Shao-Horn Y, Mallapragada DS. Role of liquid hydrogen carriers in deeply decarbonized energy systems. *ACS Sustainable Chem Eng* 2022;10:10768–80.
- [15] Distel MM, Margutti JM, Obermeier J, Nuß A, Baumeister I, Hritsyshyna M, et al. Large-Scale H₂ storage and transport with liquid organic hydrogen carrier technology: insights into Current project developments and the future outlook. *Energy Technol* 2024;2194–4288. 2301042.
- [16] Heublein N, Stelzner M, Sattelmayer T. Hydrogen storage using liquid organic carriers: equilibrium simulation and dehydrogenation reactor design. *Int J Hydrogen Energy* 2020;45:24902–16.
- [17] Perreault P, Van Hoecke L, Pourfallah H, Kummamuru NB, Boruntea C-R, Preuster P. Critical challenges towards the commercial rollouts of a LOHC-based H₂ economy. *Curr Opin Green Sustainable Chem* 2023;41:100836.
- [18] Willner M, Preuster P, Geißelbrecht M, Wasserscheid P. Continuous dehydrogenation of perhydro benzyltoluene and perhydro dibenzyltoluene in a packed bed vertical tubular reactor – the role of LOHC evaporation. *Int J Hydrogen Energy* 2024;57:1513–23.
- [19] Geißelbrecht M, Mrusek S, Müller K, Preuster P, Bösmann A, Wasserscheid P. Highly efficient, low-temperature hydrogen release from perhydro-benzyltoluene using reactive distillation. *Energy Environ Sci* 2020;13:3119–28.
- [20] Müller K, Skeledzic T, Wasserscheid P. Strategies for low-temperature liquid organic hydrogen carrier dehydrogenation. *Energy Fuels* 2021;35:10929–36.
- [21] Stoltén D, Emonts B. *Fuel cell science and engineering: materials, processes, systems and technology*. Weinheim: Wiley-VCH; 2012.
- [22] Ichikawa M. Organic liquid carriers for hydrogen storage. In: Walker G, editor. *Solid-State hydrogen storage*. Sawston. Cambridge: Woodhead Publishing; 2008. p. 500–32.
- [23] Müller K, Thiele S, Wasserscheid P. Evaluations of concepts for the integration of fuel cells in liquid organic hydrogen carrier systems. *Energy Fuels* 2019;33: 10324–30.
- [24] Rüde T, Lu Y, Anschütz L, Blasius M, Wolf M, Preuster P, et al. Performance of continuous hydrogen production from perhydro benzyltoluene by catalytic distillation and heat integration concepts with a fuel cell. *Energy Technol* 2023;11: 2201366.
- [25] Geißelbrecht M. *Prozessintensivierung für die Wasserstofffreisetzung aus flüssigen organischen Wasserstoffträgern* [Dissertation]. Erlangen: Friedrich-Alexander-Universität Erlangen-Nürnberg (FAU) 2020.
- [26] Wang Q, Le K, Lin Y, Yin W, Lin Y, Alekseeva MV, et al. Investigation on catalytic distillation dehydrogenation of perhydro-benzyltoluene: reaction kinetics, modeling and process analysis. *Chem Eng J* 2024;482:148591.
- [27] Sakuth M, Reusch D, Janowsky R. *Reactive distillation*. Ullmann's encyclopedia of industrial chemistry. Weinheim: Wiley-VCH; 2008.
- [28] Strauch D, Weiner P, Sarma BB, Körner A, Herzinger E, Wolf P, et al. Bimetallic platinum rhodium catalyst for efficient low temperature dehydrogenation of perhydro benzyltoluene. *Catal Sci Technol* 2023.
- [29] Mahayni Y, Maurer L, Auer F, Wasserscheid P, Wolf M. Structure sensitivity of the low temperature dehydrogenation of perhydro (di)benzyltoluene on supported platinum nanoparticles. preparation 2024.
- [30] Seidel A. *Entwicklung eines technischen Platin-Trägerkatalysators zur Dehydrierung von perhydro-Dibenzyltoluol* [Dissertation]. Erlangen: Friedrich-Alexander-Universität Erlangen-Nürnberg (FAU) 2019.
- [31] Auer F. *Katalysatorentwicklung für die Dehydrierung von Perhydro-Dibenzyltoluol*. Erlangen: Friedrich-Alexander-Universität Erlangen-Nürnberg (FAU); 2019 [Dissertation].
- [32] Szesni N, Frankl F, Sturm S, Wasserscheid P, Seidel A, Boesmann A. *Platin-schalenkatalysator*. DE: Clariant International Ltd, CH; 2019.
- [33] Solymosi T. *Entwicklung eines katalytisch aktivierten Plattenwärmetauschers zur Dehydrierung von Perhydro-Dibenzyltoluol* [Dissertation]. Erlangen: Friedrich-Alexander-Universität Erlangen-Nürnberg (FAU) 2021.
- [34] Ackerman G, Faith L, Heck C, Henderson H, Ritchie A. *Hydrocarbon fuels for advanced systems Part I*. Emerville California: Shell Development Co; 1970.
- [35] Tschudin SD. *Wandreaktoren für die katalytische Dehydrierung von Methylcyclohexan Kinetik und Charakterisierung*. ETH Zurich; 1997.
- [36] Solymosi T, Auer F, Dürr S, Preuster P, Wasserscheid P. Catalytically activated stainless steel plates for the dehydrogenation of perhydro dibenzyltoluene. *Int J Hydrogen Energy* 2021;46:34797–806.
- [37] Nathrath P, Ramzi YR, Bierling M, Thiele S, Wasserscheid P, Schühle P. Highly durable spray-coated plate catalyst for the dehydrogenation of perhydro benzyltoluene. *Catal Sci Technol* 2023.
- [38] Ellenberger J, Krishna R. Counter-current operation of structured catalytically packed distillation columns: pressure drop, holdup and mixing. *Chem Eng Sci* 1999;54:1339–45.
- [39] Sundmacher K. *Reaktivdestillation mit katalytischen Füllkörperpackungen: ein neuer Prozeß zur Herstellung der Kraftstoffkomponente MTBE: technische Universität Clausthal-Zellerfeld*. 1995.
- [40] Podrebarac G, Ng FT, Rempel G. More uses for catalytic distillation. *Chem Tech* 1997;27:37–45.
- [41] Basur A, Sabde D. Chapter 4 - catalyst synthesis and characterization. In: Joshi SS, Ranade VV, editors. *Industrial catalytic processes for fine and specialty chemicals*. Amsterdam: Elsevier; 2016. p. 113–86.
- [42] Smith Jr LA. *Catalyst structure and a process for its preparation*. US1981.
- [43] Clariant-International-Ltd. *EleMax® series - catalyst for storage of hydrogen from renewable sources via liquid organic hydrogen carriers (LOHC)*. 2021.
- [44] Auer F, Blaumeiser D, Bauer T, Bösmann A, Szesni N, Libuda J, et al. Boosting the activity of hydrogen release from liquid organic hydrogen carrier systems by sulfur-additives to Pt on Alumina catalysts. *Catal Sci Technol* 2019;9:3537–47.
- [45] Schneider CA, Rasband WS, Eliceiri KW. NIH image to ImageJ: 25 years of image analysis. *Nat Methods* 2012;9:671–5.
- [46] Jorschick H, Geißelbrecht M, Eibl M, Preuster P, Bösmann A, Wasserscheid P. Benzyltoluene/dibenzyltoluene-based mixtures as suitable liquid organic hydrogen carrier systems for low temperature applications. *Int J Hydrogen Energy* 2020;45: 14897–906.
- [47] Aslam R. *Separation and characterization of liquid organic hydrogen carriers (LOHCs)*. Erlangen: Friedrich-Alexander-Universität Erlangen-Nürnberg (FAU) 2016 [Dissertation].
- [48] Virtanen P, Gommers R, Oliphant TE, Haberland M, Reddy T, Cournapeau D, et al. *SciPy 1.0: fundamental algorithms for scientific computing in Python*. *Nat Methods* 2020;17:261–72.
- [49] Kitchin J. *PyCse: first release*. v1.0 ed. Zenodo; 2015.
- [50] Catmull E, Rom R. A class of local interpolating splines. *Computer aided geometric design*. 1974. p. 317–26.
- [51] Zhao Y, Shi Y, Ye G, Zhang J, Duan X, Qian G, et al. Optimization of catalyst pellet structures and operation conditions for CO methanation. *Chin J Chem Eng* 2021; 40:106–13.
- [52] Peters W, Seidel A, Herzog S, Bösmann A, Schwiager W, Wasserscheid P. Macrokinetic effects in perhydro-N-ethylcarbazole dehydrogenation and H₂ productivity optimization by using egg-shell catalysts. *Energy Environ Sci* 2015;8: 3013–21.
- [53] Kwak Y, Moon S, Ahn C-i, Kim A-R, Park Y, Kim Y, et al. Effect of the support properties in dehydrogenation of biphenyl-based eutectic mixture as liquid organic hydrogen carrier (LOHC) over Pt/Al₂O₃ catalysts. *Fuel* 2021;284:119285.
- [54] Zakgeym D, Engl T, Mahayni Y, Müller K, Wolf M, Wasserscheid P. Development of an efficient Pt/SiO₂ catalyst for the transfer hydrogenation from perhydro-dibenzyltoluene to acetone. *Appl Catal Gen* 2022;639:118644.
- [55] Zhou Y, Qi S, Tan X, Yang B, Yi C. Regulating the Pt dispersion by increasing the specific surface area of Al₂O₃ support for perhydro-dibenzyltoluene catalytic dehydrogenation reaction. *Int J Hydrogen Energy* 2024;57:52–9.
- [56] Solymosi T, Geißelbrecht M, Mayer S, Auer M, Leicht P, Terlinden M, et al. Nucleation as rate determining step in catalytic gas generation reactions from liquid phase systems. *Sci Adv* 2022;8:eade3262.
- [57] Lee K-S, Maurya S, Kim YS, Kreller CR, Wilson MS, Larsen D, et al. Intermediate temperature fuel cells via an ion-pair coordinated polymer electrolyte. *Energy Environ Sci* 2018;11:979–87.
- [58] Venugopalan G, Chang K, Nijoka J, Livingston S, Geise GM, Barges CG. Stable and highly conductive polycation-polybenzimidazole membrane blends for intermediate temperature polymer electrolyte membrane fuel cells. *ACS Appl Energy Mater* 2020;3:573–85.
- [59] Pez GP, Scott AR, Cooper AC, Cheng H. *Hydrogen storage by reversible hydrogenation of pi-conjugated substrates*. US2004.
- [60] Sotoodeh F, Huber BJ, Smith KJ. The effect of the N atom on the dehydrogenation of heterocycles used for hydrogen storage. *Appl Catal Gen* 2012;419:67–72.
- [61] Miller C, Kaibel G. Packings for fixed bed reactors and reactive distillation. *Chem Eng Sci* 2004;59:5373–9.
- [62] Hoffmann A, Noeres C, Górak A. Scale-up of reactive distillation columns with catalytic packings. *Chem Eng Process Process Intensif* 2004;43:383–95.
- [63] Sundmacher K, Hoffmann U. Development of a new catalytic distillation process for fuel ethers via a detailed nonequilibrium model. *Chem Eng Sci* 1996;51: 2359–68.
- [64] Kang J-L, Ciou Y-C, Lin D-Y, Wong DS-H, Jang S-S. Investigation of hydrodynamic behavior in random packing using CFD simulation. *Chem Eng Res Des* 2019;147: 43–54.

- [65] Ambekar AS, Rüde U, Buwa VV. Particle-resolved simulations of local liquid spreading in packed beds: effect of wettability at varying particle size. *Phys Fluids* 2022;34:062111.
- [66] Eppinger T, Wehinger GD. A generalized contact modification for fixed-bed reactor CFD simulations. *Chem Ing Tech* 2021;93:143–53.
- [67] Ambekar AS, Singh K, Kumari A, Buwa VV. Effect of particle aspect ratio and shape on the particle-scale dynamics of gas–liquid flow through packed beds. *Ind Eng Chem Res* 2023;62:18989–9003.
- [68] Hanika J, Dropka N, Kubíček M. Mass transfer in catalyst particles of non-traditional shape. *Collect Czech Chem Commun* 1996;61:564–73.